Printed in the Republic of Korea
ANALYTICAL SCIENCE & TECHNOLOGY
Vol. 27 No. 6, 314-320, 2014
http://dx.doi.org/10.5806/AST.2014.27.6.314

Microwave-modified sol-gel preparation of $La_2(MoO_4)_3:Er^{3+}/Yb^3$ particles and their upconversion photoluminescence properties

Chang Sung Lim★

Department of Advanced Materials Science & Engineering, Hanseo University, Seosan 356-706, Korea

(Received August 27, 2014; Revised November 14, 2014; Accepted November 14, 2014)

Abstract: $La_{2-x}(MoO_4)_3:Er^{3+}/Yb^{3+}$ particles with doping concentrations of Er^{3+} and Yb^{3+} ($x = Er^{3+} + Yb^{3+}$, $Er^{3+} = 0.05$, 0.1, 0.2 and $Yb^{3+} = 0.2$, 0.45) were successfully prepared by the microwave-modified sol-gel method, and the upconversion photoluminescence properties were investigated. Well-crystallized particles, formed after heat-treatment at 900 °C for 16 h, showed a fine and homogeneous morphology with particle sizes of 2-5 μm. Under excitation at 980 nm, $La_{1.7}(MoO_4)_3:Er_{0.1}Yb_{0.2}$ and $La_{1.5}(MoO_4)_3:Er_{0.05}Yb_{0.45}$ particles exhibited a strong 525 nm emission band, a weak 550 nm emission band in the green region, and a very weak 655 nm emission band in the red region. The Raman spectra of the doped particles indicated the presence of strong peaks at higher frequencies of 752, 846, 922, 1358 and 1435 cm^{-1} and lower frequency of 314 cm^{-1} induced by the disorder of the $[MoO_4]^{2-}$ groups with the incorporation of the Er^{3+} and Yb^{3+} elements into the crystal lattice or by a new phase formation.

Key words: Microwave sol-gel, upconversion, photoluminescence, Raman spectroscopy

1. Introduction

Rare earth doped upconversion (UC) phosphors have attracted great attention because of the conversion from near infrared radiation of low energy to visible radiation of high energy. These UC photoluminescence particles have potential applications in various fields, including biomedical imaging, owing to their unique UC optical behaviors that offer improved light penetration depth, high chemical and photo stability, the absence of auto-fluorescence during imaging, sharp emission bands, and high resistance to photobleaching. These properties overcome many of the current limitations in traditional photoluminescence materials.[1-3]

It is possible for the trivalent rare earth ions in the disordered tetragonal-phase to be partially substituted by Er^{3+} and Yb^{3+} ions, these ions are effectively doped into the crystal lattices of the tetragonal phase due to the similar radii of the trivalent rare earth ions, this results in the excellent UC photoluminescence properties.[4-6] Among rare earth ions, the Er^{3+} ion is suitable for converting infrared to visible light through the UC process due to its appropriate electronic energy level configuration. The co-doped Yb^{3+} ion and Er^{3+} ion can remarkably enhance the UC efficiency for the shift from infrared to visible light

★ Corresponding author
Phone : +82-(0)41-660-1445 Fax : +82-(0)41-660-1445
E-mail : cslim@hanseo.ac.kr

due to the efficiency of the energy transfer from Yb^{3+} to Er^{3+}. The Yb^{3+} ion, as a sensitizer, can be effectively excited by an incident light source energy. This energy is transferred to the activator from which radiation can be emitted. The Er^{3+} ion activator is the luminescence center of the UC particles, while the sensitizer enhances the UC luminescence efficiency.[7-9]

Recently, rare earth activated molybdates have attracted great attention because of their spectroscopic characteristics and excellent upconversion photoluminescence properties. Several processes have been developed to prepare these rare earth doped molybdates.[10-15] Usually, molybdates are prepared by a solid-state method that requires high temperatures, a lengthy heating process and subsequent grinding, these results in a loss of the emission intensity and an increase in cost. The sol-gel process provides some advantages over the conventional solid-state method, including good homogeneity, low calcination temperature, small particle size and narrow particle size distribution optimal for good luminescent characteristics. However, the sol-gel process has a disadvantage in that it takes a long time for gelation. Compared with the usual methods, microwave synthesis has the advantages of a very short reaction time, small-size particles, narrow particle size distribution, and high purity of final polycrystalline samples. Microwave heating is delivered to the material surface by radiant and/or convection heating, which is transferred to the bulk of the material via conduction.[16,17] A microwave-modified sol-gel process is a cost-effective method that provides high homogeneity and is easy to scale-up, and it is emerging as a viable alternative approach for the quick synthesis of high-quality luminescent materials.

In this study, $La_{2-x}(MoO_4)_3:Er^{3+}/Yb^{3+}$ phosphors with doping concentrations of Er^{3+} and Yb^{3+} (x = Er^{3+} + Yb^{3+}, Er^{3+} = 0.05, 0.1, 0.2 and Yb^{3+} = 0.2, 0.45) particles were prepared by the microwave-modified sol-gel method followed by heat treatment. The synthesized particles were characterized by X-ray diffraction (XRD), scanning electron microscopy (SEM), and energy-dispersive X-ray spectroscopy (EDS). The optical properties were examined comparatively using photoluminescence (PL) emission and Raman spectroscopy.

3. Experimental

Appropriate stoichiometric amounts of $La(NO_3)_3 \cdot 6H_2O$ (99%, Sigma-Aldrich, USA), $(NH_4)_6Mo_7O_{24} \cdot 4H_2O$ (99%, Alfa Aesar, USA), $Er(NO_3)_3 \cdot 5H_2O$ (99.9%, Sigma-Aldrich, USA), $Yb(NO_3)_3 \cdot 5H_2O$ (99.9%, Sigma-Aldrich, USA), citric acid (99.5%, Daejung Chemicals, Korea), NH_4OH (A.R.), ethylene glycol (A.R.) and distilled water were used to prepare $La_2(MoO_4)_3$, $La_{1.8}(MoO_4)_3:Er_{0.2}$, $La_{1.7}(MoO_4)_3:Er_{0.1}Yb_{0.2}$ and $La_{1.5}(MoO_4)_3:Er_{0.05}Yb_{0.45}$ compounds with doping concentrations of Er^{3+} and Yb^{3+} (Er^{3+} = 0.05, 0.1, 0.2 and Yb^{3+}= 0.2, 0.45). To prepare $La_2(MoO_4)_3$, 0.4 mol% $La(NO_3)_2 \cdot 6H_2O$ and 0.17 mol% $(NH_4)_6Mo_7O_{24} \cdot 4H_2O$ were dissolved in 20 mL of ethylene glycol and 80 mL of 5M NH_4OH under vigorous stirring and heating. Subsequently, citric acid (with a molar ratio of citric acid to total metal ions of 2:1) was dissolved in 100 mL of distilled water under vigorous stirring and heating. Then, the solutions were mixed together under vigorous stirring and heating at 80-100°C. At the end, highly transparent solutions were obtained and adjusted to pH=7-8 by the addition of 8M NH_4OH. In order to prepare $La_{1.8}(MoO_4)_3:Er_{0.2}$, the mixture of 0.72 mol% $La(NO_3)_3 \cdot 6H_2O$ with 0.08 mol% $Er(NO_3)_3 \cdot 5H_2O$ was used for the creation of the rare earth solution. In order to prepare $La_{1.7}(MoO_4)_3:Er_{0.1}Yb_{0.2}$, the mixture of 0.68 mol% $La(NO_3)_3 \cdot 6H_2O$ with 0.04 mol% $Er(NO_3)_3 \cdot 5H_2O$ and 0.08 mol% $Yb(NO_3)_3 \cdot 5H_2O$ was used for the creation of the rare earth solution. In order to prepare $La_{1.5}(MoO_4)_3:Er_{0.05}Yb_{0.45}$, the rare earth containing solution was generated using 0.6 mol% $La(NO_3)_3 \cdot 6H_2O$ with 0.02 mol% $Er(NO_3)_3 \cdot 5H_2O$ and 0.18 mol% $Yb(NO_3)_3 \cdot 5H_2O$.

The transparent solutions were placed into a microwave oven operating at a frequency of 2.45 GHz with a maximum output-power of 1250 W for 30 min. The working cycle of the microwave reaction was controlled very precisely using a regime of 40 s on and 20 s off for 15 min, followed by further

treatment of 30 s on and 30 s off for 15 min. The samples were treated with ultrasonic radiation for 10 min to produce a light yellow transparent sol. After this, the light yellow transparent sols were dried at 120°C in a dry oven to obtain black dried gels. The black dried gels were grinded and heat-treated at 900°C for 16 h with 100°C intervals between 600-900°C. Finally, white particles were obtained for $La_2(MoO_4)_3$ and pink particles for the doped compositions.

The phase composition of the synthesized particles was identified using XRD (D/MAX 2200, Rigaku, Japan). The microstructure and surface morphology of the synthesized particles were observed using SEM/EDS (JSM-5600, JEOL, Japan). The PL spectra were recorded using a spectrophotometer (Perkin Elmer LS55, UK) at room temperature. Raman spectroscopy measurements were performed using a LabRam Aramis (Horiba Jobin-Yvon, France). The 514.5 nm line of an Ar ion laser was used as the excitation source, and the power on the samples was kept at 0.5 mW.

3. Results and Discussion

Fig. 1 shows the XRD patterns of the (a) JCPDS 46-0407 data of $La_2(MoO_4)_3$, the synthesized (b) $La_2(MoO_4)_3$, (c) $La_{1.8}(MoO_4)_3$:$Er_{0.2}$, (d) $La_{1.7}(MoO_4)_3$:$Er_{0.1}Yb_{0.2}$ and (e) $La_{1.5}(MoO_4)_3$:$Er_{0.05}Yb_{0.45}$ particles. The crystal structures are in good agreement with the crystallographic data of $La_2(MoO_4)_3$ (JCPDS 46-0407). The pure $La_2(MoO_4)_3$ in *Fig.* 1(b) has no impurity phases. Impurity phases were detected at 22°, 23°, 24°, 25°, 29°, 32° and 50° in *Fig.* 1(c), (d) and (e). Similar impurity phases were also observed in the case of Er^{3+}/Yb^{3+} doped $CaMoO_4$ and $SrMoO_4$ molybdates when the doping concentration of Er^{3+}/Yb^{3+} is 0.02/0.18 mol%.[18,20] The foreign reflexes marked with an asterisk in *Fig.* 1(c), (d) and (e) can be ascribed to the fact that La^{3+}, Er^{3+} and Yb^{3+} ions

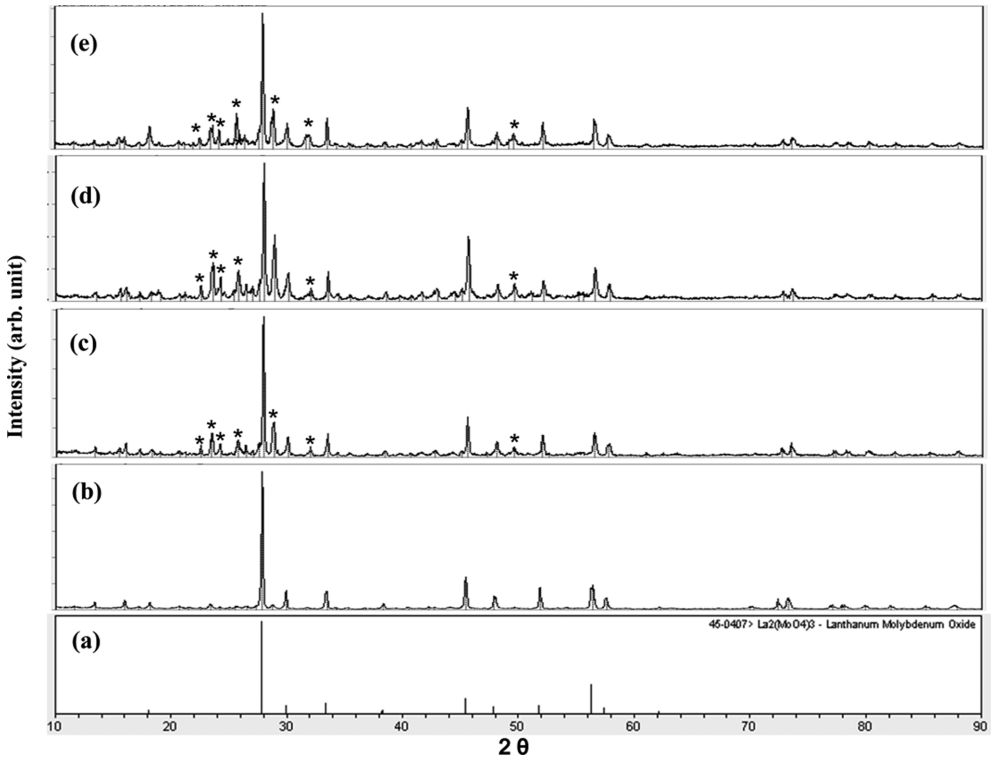

Fig. 1. X-ray diffraction patterns of the (a) JCPDS 46-0407 data of $La_2(MoO_4)_3$, the synthesized (b) $La_2(MoO_4)_3$, (c) $La_{1.8}(MoO_4)_3$:$Er_{0.2}$, (d) $La_{1.7}(MoO_4)_3$:$Er_{0.1}Yb_{0.2}$, and (e) $La_{1.5}(MoO_4)_3$:$Er_{0.05}Yb_{0.45}$ particles.

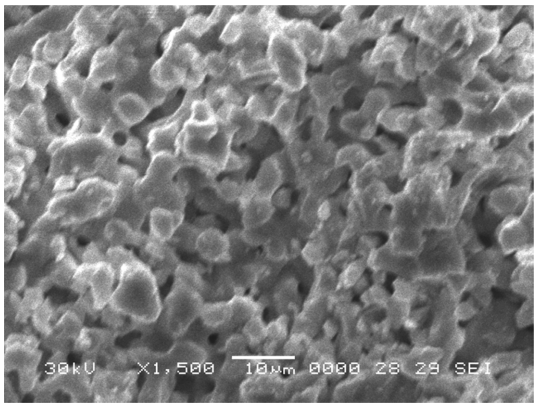

Fig. 2. Scanning electron microscopy image of the synthesized $La_{1.5}(MoO_4)_3:Er_{0.05}Yb_{0.45}$ particles.

are well substituted in the tetragonal-phase $La_{2-x}(MoO_4)_3:Er^{3+}/Yb^{3+}$ of the scheelite-type structure, and form a new phase induced by the disorder of the $[MoO_4]^{2-}$ groups.[18,20] This suggests that the microwave-modified sol-gel route is suitable for the growth of $La_{2-x}(MoO_4)_3:Er^{3+}/Yb^{3+}$ crystallites. Post heat-treatment plays an important role in a well-defined crystallized morphology. To achieve a well-defined crystalline morphology, $La_2(MoO_4)_3$, $La_{1.8}(MoO_4)_3:Er_{0.2}$, $La_{1.7}(MoO_4)_3:Er_{0.1}Yb_{0.2}$ and $La_{1.5}(MoO_4)_3:Er_{0.05}Yb_{0.45}$ phases need to be heat treated at 900°C for 16 h. It is assumed that the doping amount of Er^{3+}/Yb^{3+} has a great effect on the crystalline cell volume of the $La_2(MoO_4)_3$, because of the different ionic sizes and energy band gaps.

Fig. 2 shows a SEM image of the synthesized $La_{1.5}(MoO_4)_3:Er_{0.05}Yb_{0.45}$ particles. The as-synthesized samples are well crystallized with a fine and homogeneous morphology and particle size of 2-5 ìm. It should be noted that the sample is effectively doped into crystal lattices of the $La_2(MoO_4)_3$ phase due to the similar radii of La^{3+} and by Er^{3+} and Yb^{3+}.

Fig. 3 shows the (a) energy-dispersive X-ray

(a)

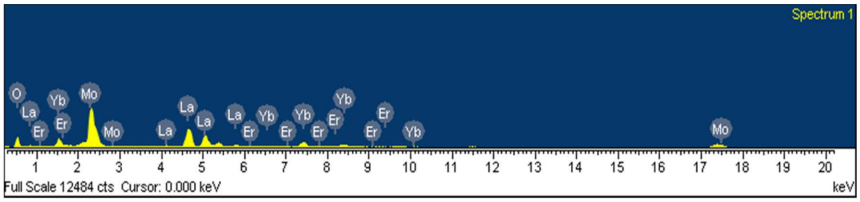

(b)

Spectrum	In stats.	O	Mo	La	Er	Yb	Total
Spectrum 1	Yes	25.03	31.95	27.07	0.43	15.53	100.00
Spectrum 2	Yes	25.97	32.23	27.02	0.81	13.97	100.00
Spectrum 3	Yes	24.24	32.06	26.56	0.48	16.66	100.00
Spectrum 4	Yes	24.48	32.63	26.70	0.55	15.64	100.00
Mean		24.93	32.22	26.84	0.56	15.45	100.00
Std. deviation		0.77	0.30	0.25	0.17	1.11	
Max.		25.97	32.63	27.07	0.81	16.66	
Min.		24.24	31.95	26.56	0.43	13.97	

(c)

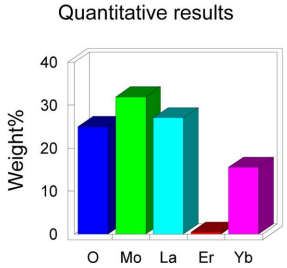

Fig. 3. Energy-dispersive X-ray spectroscopy patterns (a), quantitative compositions (b) and quantitative results (c) of the synthesized $La_{1.5}(MoO_4)_3:Er_{0.05}Yb_{0.45}$ particles.

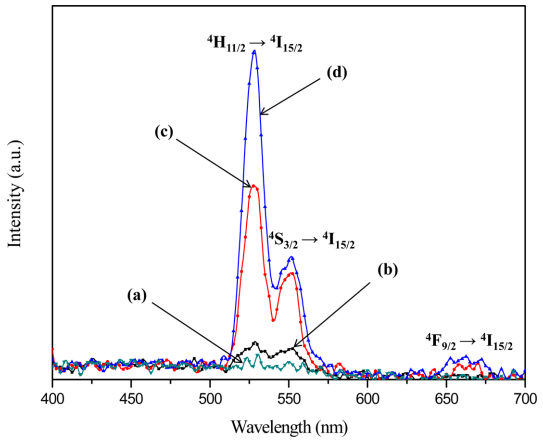

Fig. 4. Upconversion photoluminescence emission spectra of (a) $La_2(MoO_4)_3$, (b) $La_{1.8}(MoO_4)_3$:$Er_{0.2}$, (c) $La_{1.7}(MoO_4)_3$:$Er_{0.1}Yb_{0.2}$, and (d) $La_{1.5}(MoO_4)_3$:$Er_{0.05}Yb_{0.45}$ particles excited under 980 nm at room temperature.

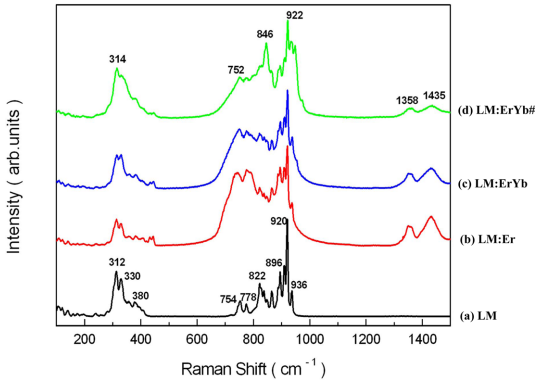

Fig. 5. Raman spectra of the synthesized (a) $La_2(MoO_4)_3$ (LM), (b) $La_{1.8}(MoO_4)_3$:$Er_{0.2}$ (LM:Er), (c) $La_{1.7}(MoO_4)_3$:$Er_{0.1}Yb_{0.2}$ (LM:ErYb) and (d) $La_{1.5}(MoO_4)_3$:$Er_{0.05}Yb_{0.45}$ (LM:ErYb#) particles excited by the 514.5 nm line of an Ar ion laser at 0.5 mW.

spectroscopy patterns, (b) quantitative compositions and (c) quantitative results of the synthesized $La_{1.5}(MoO_4)_3$:$Er_{0.05}Yb_{0.45}$ particles. The EDS pattern (a) shows that the $La_{1.5}(MoO_4)_3$:$Er_{0.05}Yb_{0.45}$ particles are composed of La, Mo, O, Er and Yb. The quantitative compositions (b) show precise constitutions of the synthesized $La_{1.5}(MoO_4)_3$:$Er_{0.05}Yb_{0.45}$ particles. The quantitative results (c) are in good relation with a nominal composition of the $La_{1.5}(MoO_4)_3$:$Er_{0.05}Yb_{0.45}$ particles. The relations between La, Mo, O, Er and Yb show that the $La_{1.5}(MoO_4)_3$:$Er_{0.05}Yb_{0.45}$ particles can be successfully synthesized using the microwave-modified sol-gel method.

Fig. 4 shows the UC photoluminescence emission spectra of the as-prepared (a) $La_2(MoO_4)_3$, (b) $La_{1.8}(MoO_4)_3$:$Er_{0.2}$, (c) $La_{1.7}(MoO_4)_3$:$Er_{0.1}Yb_{0.2}$ and (d) $La_{1.5}(MoO_4)_3$:$Er_{0.05}Yb_{0.45}$ particles excited under 980 nm at room temperature. The UC intensities of (c) $La_{1.7}(MoO_4)_3$:$Er_{0.1}Yb_{0.2}$ and (d) $La_{1.5}(MoO_4)_3$:$Er_{0.05}Yb_{0.45}$ particles exhibited a strong 525 nm emission band, a weak 550 nm emission band in the green region and a very weak 655 nm emission band in the red region. The strong 525 nm emission band and the weak 550 nm emission band in the green region correspond to the $^2H_{11/2} \rightarrow {}^4I_{15/2}$ and $^4S_{3/2} \rightarrow {}^4I_{15/2}$ transitions, respectively, while the very weak emission 655 nm band in the red region corresponds to the $^4F_{9/2} \rightarrow {}^4I_{15/2}$ transition. The UC intensities of (a) $La_2(MoO_4)_3$ was not detected. The UC intensity of (d) $La_{1.5}(MoO_4)_3$:$Er_{0.05}Yb_{0.45}$ is much higher than those of (b) $La_{1.8}(MoO_4)_3$:$Er_{0.2}$ and (c) $La_{1.7}(MoO_4)_3$: $Er_{0.1}Yb_{0.2}$ particles. Similar results are also observed from Er^{3+}/Yb^{3+} co-doped in other host matrices, which are assigned to the UC emission spectra with the green emission intensity ($^2H_{11/2} \rightarrow {}^4I_{15/2}$ and $^4S_{3/2} \rightarrow {}^4I_{15/2}$ transitions) and the red emission intensity ($^4F_{9/2} \rightarrow {}^4I_{15/2}$ transition).[7,10,18-20] The doping amounts of Er^{3+}/Yb^{3+} had a great effect on the morphological features of the particles and their UC fluorescence intensity. The Yb^{3+} ion sensitizer can be effectively excited by the energy of an incident light source, this energy is transferred to the activator where radiation can be emitted. The Er^{3+} ion activator is the luminescence center for these UC particles, and the sensitizer enhances the UC luminescence efficiency.

Fig. 5 shows the Raman spectra of the synthesized (a) $La_2(MoO_4)_3$ (LM), (b) $La_{1.8}(MoO_4)_3$:$Er_{0.2}$ (LM:Er), (c) $La_{1.7}(MoO_4)_3$:$Er_{0.1}Yb_{0.2}$ (LM:ErYb), and (d) $La_{1.5}(MoO_4)_3$:$Er_{0.05}Yb_{0.45}$ (LM:ErYb#) particles excited by the 514.5 nm line of an Ar ion laser at 0.5 mW. The internal modes for the well-resolved sharp peaks for the $La_2(MoO_4)_3$ particles indicate a high crystallinity state of the synthesized particles. The internal vibration mode frequencies are dependent on the lattice

parameters and the degree of the partially covalent bond between the cation and molecular ionic group $[MoO_4]^{2-}$. The Raman spectra of the (b) $La_{1.8}(MoO_4)_3$:$Er_{0.2}$ (LM:Er), (c) $La_{1.7}(MoO_4)_3:Er_{0.1}Yb_{0.2}$ (LM:ErYb), and (d) $La_{1.5}(MoO_4)_3:Er_{0.05}Yb_{0.45}$ (LM:ErYb#) particles indicate the domination of strong peaks at higher frequencies of 752, 846, 922, 1358 and 1435 cm^{-1} and lower frequency of 314 cm^{-1}. The Raman spectra of the doped particles prove that the doping ions can influence the structure of the host materials. The combination of a heavy metal cation and the large inter-ionic distance for Er^{3+} and Yb^{3+} substitutions in La^{3+} sites in the lattice result in a high probability of UC and phonon-splitting relaxation in $La_{2-x}(MoO_4)_3$ crystals. It may be that these very strong and strange effects are generated by the disorder of the $[MoO_4]^{2-}$ groups with the incorporation of the Er^{3+} and Yb^{3+} elements into the crystal lattice or by a new phase formation.

4. Conclusions

The $La_{2-x}(MoO_4)_3:Er^{3+}/Yb^{3+}$ particles with doping concentrations of Er^{3+} and Yb^{3+} were successfully synthesized by the microwave-modified sol-gel method. Well-crystallized particles formed after heat-treatment at 900 °C for 16 h showed a fine and homogeneous morphology with particle sizes of 2-5 μm. Under excitation at 980 nm, the UC intensities of $La_{1.7}(MoO_4)_3:Er_{0.1}Yb_{0.2}$ and $La_{1.5}(MoO_4)_3:Er_{0.05}Yb_{0.45}$ particles exhibited a strong 525 nm emission band and a weak 550 nm emission band in the green region, which were assigned to the $^2H_{11/2}\rightarrow{}^4I_{15/2}$ and $^4S_{3/2}\rightarrow{}^4I_{15/2}$ transitions, respectively, while a very weak 655 nm emission band in the red region was assigned to the $^4F_{9/2}\rightarrow{}^4I_{15/2}$ transition. The UC intensity of $La_{1.5}(MoO_4)_3:Er_{0.05}Yb_{0.45}$ particles was much higher than that of the $La_{1.8}(MoO_4)_3:Er_{0.2}$ and $La_{1.7}(MoO_4)_3:Er_{0.1}Yb_{0.2}$ particles. The Raman spectra of the $La_{1.8}(MoO_4)_3:Er_{0.2}$, $La_{1.7}(MoO_4)_3:Er_{0.1}Yb_{0.2}$, and $La_{1.5}(MoO_4)_3:Er_{0.05}Yb_{0.45}$ particles indicated the domination of strong peaks at higher frequencies of 752, 846, 922, 1358 and 1435 cm^{-1} and lower frequency of 314 cm^{-1} induced by the disorder of the $[MoO_4]^{2-}$ groups with the incorporation of the Er^{3+} and Yb^{3+} elements into the crystal lattice or by a new phase formation.

Acknowledgements

This study was supported by the Basic Science Research Program through the National Research Foundation of Korea (NRF) funded by the Ministry of Science, ICT & Future Planning (2014-046024).

References

1. M. Wang, G. Abbineni, A. Clevenger, C. Mao and S. Xu, *Nanomedicine: NBM,* **7**, 710-729 (2011).
2. Y. J. Chen, H. M. Zhu, Y. F. Lin, X. H. Gong, Z. D. Luo and Y. D. Huang, *Opt. Mat*., **35**, 1422-1425 (2013).
3. M. Lin, Y. Zho, S. Wang, M, Liu, Z. Duan, Y. Chen, F. Li, F. Xu and T. Lu, *Bio. Adv*., **30**, 1551-1561 (2012).
4. J. Liao, D. Zhou, B. Yang, R. Liu, Q. Zhang and Q. Zhou, *J. Lum*., **134**, 533-538 (2013).
5. J. Sun, Y. Lan, Z. Xia and H. Du, *Opt. Mat*., **33**, 576-581 (2011).
6. C. Guo, H. K. Yang and J. H. Jeong, *J. Lum*., **130**, 1390-1393 (2010).
7. J. Sun, J. Xian and H. Du, *J. Phys. Chem. Sol*., **72**, 207-213 (2011).
8. V. K. Komarala, Y. Wang and M. Xiao, *Chem. Phys. Lett*., **490**, 189-193 (2010).
9. J. Sun, J. Xian, Z. Xia and H. Du, *J. Rare Earths*, **28**, 219-221 (2010).
10. L. Qin, Y. Huang, T, Tsuboi and H. J. Seo, *Mat. Res. Bull*., **47**, 4498-4502 (2012).
11. Y. L. Yang, X. M. Li, W. L. Feng, W. L. Li and C. Y. Tao, *J. Alloys Comps*., **505**, 239-242 (2010).
12. Y. Huang, L. Zhou and Z. Tang, *Opt. Mat*., **33**, 777-782 (2011).
13. Y. Tian, B. Chen, B. Tian, J. Sun, X. Li, J. Zhang, L. Cheng, H. Zhong, H. Zhong, Q. Meng and R. Hua, *Physica B*, **407**, 2556-2559 (2012).
14. Q. Chen, L. Qin, Z. Feng, R. Ge, X. Zhao and H. Xu, *J. Rare Earths*, **29**, 843-848 (2011).
15. J. Zhang, X. Wang, X, Zhang, X. Zhao, X. Liu and L. Peng, *Inog. Chem. Comm*., **14**, 1723-1727 (2011).

16. C. S. Lim, *Mat. Chem. Phys.*, **140**, 154-158 (2013).
17. S. Das, A. K. Mukhopadhyay, S. Datta and D. Basu, *Bull. Mat. Sci*., **32**, 1-13 (2009).
18. C. S. Lim, *Mat. Res. Bull*., **47**, 4220-4225 (2012).
19. W. Lu, L. Cheng, J. Sun, H. Zhong, X. Li, Y. Tian, J. Wan, Y. Zheng, L. Huang, T. Yu, H. Yu and B. Chen, *Physica B*, **405**, 3284-3288 (2010).
20. C. S. Lim, *Mat. Res. Bull*., **48**, 3805-3810 (2013)
21. J. Sun, B. Sue and H. Du, *Infrar. Phys. Tech*., **60**, 10-14 (2013).
22. Q. Sun, X. Chen, Z. Liu, F. Wang, Z. Jiang and C. Wang, *J. Alloys Comps*., **509**, 5336-5340 (2012).